Process Safety and Environmental Protection 173 (2023) 75–87

Contents lists available at ScienceDirect

Process Safety and Environmental Protection

journal homepage: www.journals.elsevier.com/process-safety-and-environmental-protection

Co-pyrolysis of biosolids with lignocellulosic biomass: Effect of feedstock on product yield and composition

Nimesha Rathnayake [a], Savankumar Patel [a,b], Ibrahim Gbolahan Hakeem [a,b], Jorge Pazferreiro [a], Abhishek Sharma [a,b,c], Rajender Gupta [d], Catherine Rees [e], David Bergmann [f], Judy Blackbeard [e], Aravind Surapaneni [b,e], Kalpit Shah [a,b,*]

[a] Chemical & Environmental Engineering, School of Engineering, RMIT University, Melbourne, Victoria 3000, Australia
[b] ARC Training Centre on Advance Transformation of Australia's Biosolids Resources, RMIT University, Bundoora, Victoria 3083, Australia
[c] Department of Chemical Engineering, Manipal University Jaipur, Jaipur, Rajasthan 303007, India
[d] Department of Chemical & Materials Engineering, University of Alberta, Edmonton, Alberta, Canada
[e] Melbourne Water, Docklands, Victoria 3008, Australia
[f] South East Water, Frankston, Victoria 3199, Australia

ARTICLE INFO

Keywords:
Biosolids
Lignocellulosic biomass
Co-pyrolysis
Biochar

ABSTRACT

Co-pyrolysis technology is an effective method to reduce heavy metal concentration in biochar produced from biosolids. In the current study, the effect of co-pyrolysis feedstock on product yield and properties was studied by mixing Biosolids (BS) with Wheat Straw (WS) and Canola Straw (CS) in a 3:1 mass ratio and carrying out thermal decomposition at 700 °C in a fluid bed reactor. This study found that the feedstock ash content and the volatile matter had a significant effect on biochar, oil, and gas yields from co-pyrolysis. The results also indicated that the addition of WS and CS feedstock notably reduced As, Cd, Cr, Cu, Ni, Pb, Se, and Zn concentrations in the biochar, due to the net effect of dilution and synergistic effects. BS-WS and BS-CS co-pyrolysis reduced Cu concentration in biochar by 61.6% and 63.3%, respectively, and Zn concentration by 66.4% and 64.4%, respectively. Lignocellulosic biomass addition also reduced biochar yield and improved C, H, and N content, along with the calorific value and the thermal stability of biochar. C content was increased by 36.9% in BS: WS biochar and 43.3% in BS: CS biochar compared to solely biosolids' biochar. The calorific value of biochar was increased by 43.5% and 52.9% in BS-WS biochar and BS-CS biochar compared to biosolids' biochar. During co-pyrolysis, CS addition produced oil with the lowest mole percentage of nitrogenated compounds. However, the addition of WS and CS increased co-pyrolysis oil acidity. Biosolids co-pyrolysis with WS and CS also increased the gas yield and the heating value compared to biosolids pyrolysis. Furthermore, the synergistic effect between biosolids and co-feedstocks resulted in increased gas yields and decreased oil and biochar yields.

1. Introduction

In recent years, transforming biosolids to biochar by pyrolysis has been studied extensively as a sustainable method to manage biosolids (Fonts et al., 2012; Inguanzo et al., 2002; McNamara et al., 2016; Patel et al., 2019; Singh and Agrawal, 2008; Song et al., 2014). Pyrolysis of biosolids has demonstrated the potential to eliminate most of the contaminants present in biosolids, such as odor, disease-causing organisms, micro-plastics, pesticides, and pharmaceutical-related impurities, and to partially destroy Per- and Polyfluoroalkyl Substances (PFAS) present in biosolids (Fonts et al., 2012; Inguanzo et al., 2002; McNamara et al., 2016; Patel et al., 2019; Singh and Agrawal, 2008; Song et al., 2014). However, biochar produced from biosolids pyrolysis has limitations due to its high heavy metal concentration, low carbon content, and low calorific value (Patel et al., 2020; Yang et al., 2018).

Co-pyrolysis demonstrates extraordinary potential as a developing technique to upgrade biochar properties and increase its potential in agricultural and non-agricultural applications (Singh and Agrawal, 2008; Patel et al., 2020; Abnisa and Wan, 2014; Wang et al., 2016a, 2020; Zhao et al., 2017). Co-pyrolysis involves blending biosolids with another feedstock and heating the blend in an inert environment. It is more economical and efficient than other alternatives, such as acid

* Corresponding author at: Chemical & Environmental Engineering, School of Engineering, RMIT University, Melbourne, Victoria 3000, Australia.
E-mail address: kalpit.shah@rmit.edu.au (K. Shah).

https://doi.org/10.1016/j.psep.2023.02.087
Received 15 November 2022; Received in revised form 1 February 2023; Accepted 28 February 2023
Available online 4 March 2023

treatment and metal extraction (Veeken, 1999; Marinos et al., 2007).

Recently, many researchers have studied the co-pyrolysis of biosolids, and they mainly focussed on the yield distribution, biochar properties, and the presence of synergistic effects under different temperatures and mixing ratios (Wang et al., 2020, 2018, 2016b; Zhao et al., 2017; Ali et al., 2022; Bai et al., 2021; Dong et al., 2019; Han et al., 2013; Huang et al., 2017; Jin et al., 2018; Lin et al., 2016; Martínez et al., 2014; Saleh Khodaparasti et al., 2022; Urych and Smoliński, 2021, 2019; Zhang et al., 2020; Zhu et al., 2014; Shuang-quan et al., 2009). These studies have observed that the temperature and mixing ratio of the process had significant effects on yield distribution, biochar properties, and their potential agronomic and environmental values for enhancing soil quality (Wang et al., 2020, 2019; Dong et al., 2019; Huang et al., 2017; Jin et al., 2017). Most of those studies have used lignocellulosic biomass co-feedstocks such as cotton stalk, rice straw, rice husk, wheat straw, pinewood, and bamboo sawdust due to their abundance and low cost (Wang et al., 2016a, 2019; Huang et al., 2017, 2016b; Jin et al., 2017; Alvarez et al., 2015; Lan et al., 2020; Zhang et al., 2015a; Zhu et al., 2018).

Several co-pyrolysis studies have observed that co-pyrolysis behavior is not a simple summation calculation, and there are synergistic effects when co-pyrolysis is carried out in TGA and fixed bed reactors (Shuang-quan et al., 2009; Wang et al., 2016b; Jin et al., 2017). Wang et al., 2016, Alvarez et al., 2015 and Zuo et al., 2014 observed that with the addition of biomass wastes (Wheat straw, Pinewood sawdust), co-pyrolysis of biosolids produced higher gas and liquid yield and lower biochar yield than the expected yield values (Wang et al., 2016b; Alvarez et al., 2015; Zuo et al., 2014). However, Zhu et al., 2015 reported observing no synergistic effects between biosolids and pine sawdust in a thermogravimetric reactor at 1000 °C (Zhu et al., 2014). Therefore, statements regarding synergistic effects are still not conclusive, and further investigations on synergistic effects with different co-feedstock types, operating conditions, and reactor types are crucial for establishing the mechanisms of synergistic effects.

The type of co-pyrolysis reactor used has a critical effect on the co-pyrolysis behavior since the contact between particles, heat transfer characteristics, and volatile residence time depends on the reactor type used in the pyrolysis/co-pyrolysis reactor (Abnisa and Wan, 2014; Fadhilah et al., 2023). However, most of the co-pyrolysis of biosolids studies in the literature were performed in TGA or fixed bed-type reactors. Several comprehensive reviews comparing the pyrolysis reactor types show that product yield distribution heavily depends on the type of reactor used (Dong et al., 2019; Han et al., 2013; Huang et al., 2017; Lin et al., 2016; Wang et al., 2019; Ischia et al., 2011; Ruiz-Gomez et al., 2017). Fluidized bed reactors demonstrated rapid heat transfer, enhanced control of temperature and residence time, and improved mixing of particles compared to other reactor types (Abnisa and Wan, 2014; Fadhilah et al., 2023). Furthermore, fluidized bed reactors are beneficial because of their ease of scalability, ability to process materials with a broad particle size distribution, and simple operation (McNamara et al., 2016; Zuo et al., 2014; Ruiz-Gomez et al., 2017). In addition, Fei et al. noted that the extent of contact between feedstock particles in the reactor is an essential parameter that can induce synergy (Fei et al., 2012). Therefore, it can be hypothesized that fluidized bed reactors may improve synergistic effects in co-pyrolysis because of the higher mixing and improved contact between particles (Fadhilah et al., 2023). However, the co-pyrolysis of biosolids with lignocellulosic biomass in a fluidized bed reactor has not been studied. Therefore, it is crucial to investigate the co-pyrolysis behavior in a fluid bed setting and investigate the presence of synergistic effects.

Moreover, most biosolids co-pyrolysis studies published in the literature focused on understanding synergetic effects and biochar product characterization (Wang et al., 2020, 2019; Ali et al., 2022; Huang et al., 2017; Zhang et al., 2020; Jin et al., 2017; Fan et al., 2016). As a result, studies on the properties of co-pyrolysis oil and gas products are fewer since biochar was focused on as the main product. Nevertheless, investigating the properties of co-pyrolysis oil and gas products is vital as large-scale pyrolysis plants may use oil and gas vapors for bioenergy generation, and the synergetic effect of co-pyrolysis may improve oil and gas vapors yield, composition, and other critical physicochemical properties for bioenergy generation (McNamara et al., 2016; PYREG GmbH, 2018).

On this basis, the current study aims to (a) investigate the effect of feedstock properties on co-pyrolysis behavior and product (biochar, oil, and gas) properties and (b) study the synergistic effect on yield distribution, oil and gas properties, and heavy metal concentration in biochar, in a fluidized bed reactor. Lignocellulosic biomasses were selected as the co-feedstocks in the current study due to their low ash, heavy metal, and high carbon content. Therefore, blending lignocellulosic biomass with biosolids (BS) is hypothesized to produce biochar with improved carbon content, surface area, and low heavy metal content. Wheat straw (WS) and canola straw (CS) were selected as the co-feedstocks in the current study. The selection of these lignocellulosic biomasses was based on mapping of agricultural waste generation in Victoria, Australia, as per the availability, cost, physicochemical properties (Ultimate and proximate analysis, and total heavy metal content), and proximity to wastewater treatment facilities. The mapping study results are included in the supplementary document (Fig. S1) (Department of Agriculture, 2019; Department of Economic Development, J., Transport and Resources, 2014; Mark Siebentritt and Associates, G.O.P.L., Renewable Energy Production from Almond Waste, 2012; Melissa Morris, 2010; Statistics, 2019). In addition, co-pyrolysis results of biosolids with WS and CS were compared with co-pyrolysis results of biosolids and alum sludge from a previous study (Rathnayake et al., 2022) carried out by our research group to analyze the effect of feedstock type on the decomposition behavior.

2. Materials and methods

Biosolids (BS) samples were collected from the Mount Martha Water Recycling Plant of South East Water Corporation in Victoria, Australia. Wheat straw (WS) and canola straw (CS) samples were collected from Buloke Park Farms, Bridgewater, Victoria, and Yarrawonga, Victoria. These samples were ground and sieved to achieve the desired particle size range (100–300 μm) using a ring mill and an automatic sieve shaker. All the samples were dried in the oven for 24 h at 105 °C (Binder FED 720 drying oven, Binder GmbH, Germany).

Pyrolysis and co-pyrolysis experiments were performed in a quartz tube fluidized bed reactor with a 27 mm inner diameter and a reaction zone with a height of 680 mm (Patel et al., 2019; Rathnayake et al., 2022). The ceramic frit distributor plate with a porosity of 3 (16 −40 μm) is placed at a 320 mm distance from the bottom of the reactor to ensure that the gas was sufficiently preheated before entering the reaction zone (Patel et al., 2019; Rathnayake et al., 2022). The diagram of the experimental setup is included in the supplementary materials (Fig. S2), and further information on the reactor specifications can be found in a previous study carried out by our research group (Patel et al., 2019; Rathnayake et al., 2022). Initially, the feed sample was loaded into the reactor, and nitrogen was flushed through the setup for around 15 min to ensure an inert atmosphere. Then the reactor was heated to the required temperature (700 °C) using an electric furnace (Gradient Tube Furnace, Carbolite EZS-3 G, UK) at 35 °C/min while continuously feeding nitrogen to maintain minimum fluidization velocity. After achieving the required furnace temperature (700 °C), it was maintained for one hour. The outlet gas stream was analyzed using an Agilent Micro GC 490 (GC, Agilent Micro GC 490, USA) connected to the reactor system. Micro GC extracted gas samples from the outlet gas stream every 4 min for analysis. After each experimental run, the reactor system was allowed to cool down to room temperature before collecting biochar and oil samples. Biochar was collected from the reactor, and pyrolysis oil was extracted from the condensers using dichloromethane.

Co-pyrolysis experiments of BS with WS and CS were carried out at a

3:1 mixing ratio and 700 °C. This temperature and mixing ratio were selected based on optimum process conditions identified by the previous co-pyrolysis study carried out by our group (Rathnayake et al., 2022). Every experiment was replicated three times to improve the reproducibility of the data. Biochar(BC) samples from pyrolysis experiments of biosolids, wheat straw, and canola straw were labeled as BSBC, WSBC, and CSBC, and from biochar co-pyrolysis of biosolids with wheat straw and canola straw were labeled as WS: BSBC and CS: BSBC, respectively.

The mass of biochar produced was calculated by subtracting the initial weight of the reactor (including the feedstock sample) from the weight of the reactor after the experiment (including biochar produced). The mass of bio-oil produced was calculated by subtracting the initial weight of the condensers and tubing from the weight of the condensers and tubing after the experiment.

$$Biochar\ mass\ yield(\%) = \frac{Mass\ of\ biochar/oilproduct}{Mass\ of\ feedstock\ used\ in\ pyrolysis/co-pyrolysis} \times 100 \quad (1)$$

$$Oil\ mass\ yield(\%) = \frac{Mass\ of\ biochar/oil\ product}{Mass\ of\ feedstock\ used\ in\ pyrolysis/co-pyrolysis} \times 100 \quad (2)$$

Biochar and oil yields were calculated by Eq. (1) and (2), respectively, and gas mass yield was calculated by the difference as shown in Eq. (3);

$$Pyrolysis\ gas\ mass\ yield(\%) = 100 - Biochar\ mass\ yield(\%) - Pyrolysis\ oil\ mass\ yield(\%) \quad (3)$$

Heavy metals (As, Cd, Cr, Cu, Ni, Pb, Se, and Zn) in the biochar and the feed materials were determined using an inductively coupled plasma optical emission spectrometry (ICP-MS; Optima 5300DV; Perkin Elmer, USA). Before ICP-MS analysis, samples were digested following the US EPA 3050B method (Wang et al., 2018). Bioavailable fractions of selected heavy metals (Cd, Cu, Ni, Pb, and Zn were determined by the DTPA extraction method as described in Lindsay and Norvell (1978), followed by ICP-MS analysis (Wang et al., 2019). Proximate and Ultimate analysis of original feedstock and biochar were determined using a thermogravimetric analyzer (TGA, TGA Q500 IR, USA) and an elemental analyzer (CHNS analyzer, Perkin Elmer 2400 Series II CHNS/O, USA). A Bomb calorimeter (Automatic Calorimeter 6400 Parr, USA) was used to determine the calorific value of biochar. A Fourier Transform Infrared Spectometer (FT-IR, Perkin Elmer Spectrum 100, USA) for the wavenumbers ranging from 4000 to 600 cm^{-1} with 32 scans at 4 cm^{-1} resolution Brunauer–Emmett–Teller (BET) surface area of the biochar samples were determined using a surface area analyzer (High Throughput Surface Area and Porosity Analyzer, TriStar II 3020, UK) and degasser (Degasser, VacPrep™ 061, UK). Surface characteristics of biochar were further analyzed using Scanning Electron Microscopy (SEM, FEI Quanta 200, Sweden) imaging.

Oil samples were analyzed using Gas chromatography–Mass spectrometry (GC/MS, Agilent, GC-7890A, and MS-5975 C, USA) to determine the relative composition of components in oil. Further details on the temperature program and the column specifications can be found in a previous study (Rathnayake et al., 2022). In addition, pH levels in bio-oil samples were checked using a calibrated pH meter (Benchtop pH meter, Thermo Scientific Orion 3 Star, USA). In between the measurements, the probe of the pH meter was rinsed with isopropyl alcohol, followed by DI water, to remove any residue.

Synergistic effects during co-pyrolysis of biosolids with different feedstocks in yield distribution were investigated by comparing the experimentally derived parameters with the calculated ones. The latter were obtained by applying the rule of mixtures. By this means, the behavior is derived from a linear interpolation of the yields of the pure feedstocks. The calculated yields for co-pyrolysis were obtained from Eq. (4), shown below;

$$Y_{i,calculated} = \frac{Y_{i,BS} + 3 \times Y_{i,F}}{4} \quad (4)$$

Where $Y_{i,calculated}$ is the calculated mass yield of i pyrolysis product (biochar, oil, or gas) in co-pyrolysis. $Y_{i,BS}$ is the experimental mass yield of i in, and $Y_{i,F}$ is the experimental mass yield of i in WS or CS.

The pyrolysis gas's higher heating value (HHV) is calculated by Eq. (5)below, where φ_i is the average molar percentages of CO, H_2, CH_4, C_2H_6, and C_3H_8 (Zhang et al., 2020).

$$HHV\left(MJ/Nm^3\right) = \frac{(\varphi_{CO} \times 12.633) + (\varphi_{H_2} \times 12.745) + (\varphi_{CH_4} \times 39.819) + (\varphi_{C_2H_6} \times 63.414) + \left(\varphi_{C_3H_8} \times 101.242\right)}{100} \quad (5)$$

SPSS 15.0 was used to analyze yield distribution from experiments accounting for the effects of co-pyrolysis feedstock. In addition, Turkey's test was used to differentiate means within treatments ($P < 0.05$). Results from this analysis are included in supplementary data (Table S2).

3. Results and discussion

3.1. Product yield

Biochar, oil, and gas product yields from different pyrolysis and co-pyrolysis experiments are shown in Fig. 1. Pyrolysis of WS and CS resulted in lower biochar yields and higher oil and gas yields compared to pyrolysis of BS. The lower ash content in WS and CS compared to BS can explain these results (See Table 1) since many studies have observed that the ash content present in the feed positively correlates with the biochar yield (Huang et al., 2017; Zhu et al., 2018; Suliman et al., 2016). Furthermore, high oil and gas yields from WS and CS are connected to high volatile matter content in the raw feed materials. Thus, high volatile matter and low ash content in WS and CS feed explain the higher oil and gas yields from lignocellulosic biomass (WS and CS) pyrolysis compared to BS (See Table 1).

The differences in CS and WS pyrolysis product distribution can be attributed to the differences in their chemical composition. In literature, cellulose, hemicellulose, and lignin composition in WS were reported as 42–50%, 23–30%, and 16–18%, respectively, and in CS, it was reported as 34–36%, 14–16% and 24–27% (Adapa et al., 2009; Adapa and Schoenau, 2009; Ji et al., 2014; Wenchao Ji et al., 2014; Fajardo and E. C.M, 2015; Fragiskos et al., 2014). Therefore, higher biochar yield from WS pyrolysis can be linked to the higher lignin content in WS compared to CS, and higher gas content in CS pyrolysis can be linked to higher hemicellulose in CS compared to WS (Batista and Gomes, 2021; Shahbaz et al., 2020).

In co-pyrolysis experiments, adding CS and WS reduced biochar yield by 46.72% and 43.82%, respectively, and increased gas yield by 79.53% and 92.34%, respectively, compared to BS pyrolysis (See Fig. 1). On the other hand, oil yield in WS and CS co-pyrolysis experiments remained in the 40–42% range, which was comparable to BS pyrolysis (See Fig. 1).

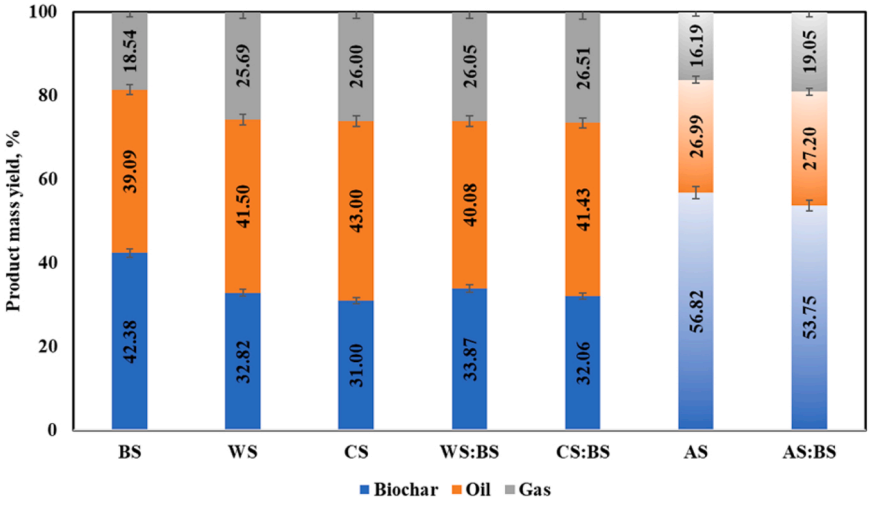

Fig. 1. Product mass yield of biochar, oil, and gas products from pyrolysis/co-pyrolysis of biosolids, alum sludge, wheat straw, and canola straw (Rathnayake et al., 2022). BS-Biosolids pyrolysis, AS-Alum sludge pyrolysis, WS-Wheat straw pyrolysis, CS- Canola straw pyrolysis, AS:BS-Alum sludge and biosolids co-pyrolysis at 3:1, WS:BS-Wheat straw and biosolids co-pyrolysis at 3:1, CS:BS-Canola straw and biosolids co-pyrolysis at 3:1.

Table 1
Ultimate and Proximate analysis of feedstock and resultant biochar from pyrolysis co-pyrolysis experiments on a dry basis (Rathnayake et al., 2022).

Samples		Feedstocks			Pyrolysis biochar			Co-pyrolysis biochar		AS co-pyrolysis data		
		BS	WS	CS	BSBC	WSBC	CSBC	WS: BS BC	CS: BS BC	AS	ASBC	AS: BS BC
Ultimate analysis (wt%)	C	36.71 ± 1.39	46.41 ± 5.32	50.36 ± 3.48	26.46 ± 0.67	38.51 ± 3.77	40.91 ± 3.77	36.22 ± 4.46	37.92 ± 1.12	12.18 ± 0.59	10.44 ± 0.06	12.51 ± 0.97
	H	4.24 ± 0.58	3.12 ± 1.43	3.98 ± 0.57	1.03 ± 0.05	1.27 ± 0.29	1.46 ± 0.29	1.91 ± 0.08	2.03 ± 0.12	5.82 ± 0.17	2.16 ± 0.70	0.19 ± 0.40
	N	5.42 ± 0.46	1.43 ± 0.98	2.95 ± 0.58	3.33 ± 0.16	0.63 ± 0.43	0.82 ± 0.43	1.92 ± 0.24	2.15 ± 1.03	1.26 ± 0.13	0.99 ± 0.10	1.13 ± 0.05
	S	0.92 ± 0.09	0.06 ± 0.92	0.07 ± 0.17	0.52 ± 0.03	0.23 ± 0.12	0.19 ± 0.12	0.10 ± 0.06	0.15 ± 0.13	0.68 ± 0.18	0.32 ± 0.07	0.42 ± 0.06
	O[a]	23.70 ± 0.89	44.41 ± 0.92	37.53 ± 2.57	8.35 ± 0.67	18.09 ± 1.68	17.21 ± 4.30	13.58 ± 5.83	12.74 ± 2.01	23.06 ± 0.31	9.55 ± 0.48	9.12 ± 2.28
H/C		1.39	0.81	0.95	0.47	0.40	0.43	0.63	0.64	5.73	2.48	0.18
O/C		0.48	0.72	0.56	0.24	0.35	0.32	0.28	0.25	1.42	0.69	0.55
HHV (MJ/kg)		14.68 ± 0.24	17.22 ± 4.51	19.17 ± 3.89	9.17 ± 0.31	14.41 ± 4.06	15.53 ± 4.64	13.16 ± 6.89	14.02 ± 5.58	8.81 ± 0.42	5.51 ± 0.90	2.69 ± 1.15
Proximate analysis (wt%)	Volatile Matter	55.7 ± 1.00	74.04 ± 5.43	70.12 ± 1.67	12.11 ± 3.00	30.58 ± 1.47	30.22 ± 1.14	34.34 ± 4.03	34.22 ± 1.22	27.12 ± 0.34	10.79 ± 0.88	10.28 ± 0.58
	Ash	28.43 ± 0.29	4.57 ± 1.49	5.11 ± 1.23	60.30 ± 0.04	41.27 ± 3.24	39.41 ± 3.65	46.27 ± 1.65	45.01 ± 2.34	56.23 ± 0.29	76.54 ± 1.20	76.63 ± 0.73
	Fixed Carbon	15.81 ± 1.29	21.39 ± 4.11	24.77 ± 3.21	27.59 ± 3.11	28.15 ± 3.22	30.37 ± 2.89	19.39 ± 3.54	20.77 ± 2.89	16.65 ± 0.05	12.67 ± 2.08	13.09 ± 0.15

BS-Biosolids, AS-Alum sludge, WS- Wheat straw, CS- Canola straw, BSBC- Biosolids' biochar, ASBC-Alum sludge biochar, WSBC-Wheat straw biochar, CSBC- Canola straw biochar, AS:BSBC- Biochar derived from alum sludge and biosolids co-pyrolysis at 3:1, WS:BSBC- Biochar derived from wheat straw and biosolids co-pyrolysis at 3:1, CS:BSBC- Biochar derived from canola straw and biosolids co-pyrolysis at 3:1

[a] Calculated by the difference

The addition of lignocellulosic biomass (WS and CS) increases the volatile matter content and reduces the feed blend's overall ash content, which explains the higher gas yield and the lower biochar yield in co-pyrolysis compared to pyrolysis of BS (Wang et al., 2020, 2019; Dong et al., 2019).

Tar produced from pyrolysis and co-pyrolysis of biosolids and biomass contains a diverse and complicated mixture of various organic compounds, such as oxygen-containing hydrocarbons, aromatic compounds, sulfur-containing hydrocarbons, and aromatic hydrocarbons (Alen Horvat and Tar, 2019). Tar cracking reactions, as shown in Eq. (6), (7), and (8) below, decompose heavy molecular weight hydrocarbon compounds to form low molecular weight gaseous compounds such as CO, CH_4, and H_2. Minerals in biosolids such as Mg_2SiO_4, CaO, $CaCO_3$, $MgCO_3$, Fe_2SiO_4, clay minerals, and alkali metals act as catalysts to promote tar-cracking reactions (Zhu et al., 2018; Yang et al., 2015).

$$C_xH_y + CO_2 \rightarrow \frac{y}{2}H_2 + 2xCO \quad (6)$$

$$C_xH_y + 2H_2O \rightarrow \left(x + \frac{y}{2}\right)H_2 + xCO \quad (7)$$

$$C_xH_y + \frac{2x - y}{2}H_2 \rightarrow xCH_4 \quad (8)$$

It is also essential to compare the behavior of adding lignocellulosic biomass (CS and WS) with other feedstock types, such as sludge waste. In the current study, WS and CS co-pyrolysis data were compared with the results of alum sludge (AS) pyrolysis/co-pyrolysis, and the required data was taken from our previous study (Rathnayake et al., 2022) AS behaved similarly to BS during pyrolysis and produced high biochar yield and low oil and gas yield. This behavior is consistent with the literature and can be explained by high ash content and low volatile matter in AS and BS (See Fig. 1) (Patel et al., 2019; Singh and Agrawal, 2008; Huang et al., 2017; Jin et al., 2017; Ruiz-Gomez et al., 2017).

Moreover, significant differences in yield distribution could be observed between AS and lignocellulosic biomass (WS and CS) co-

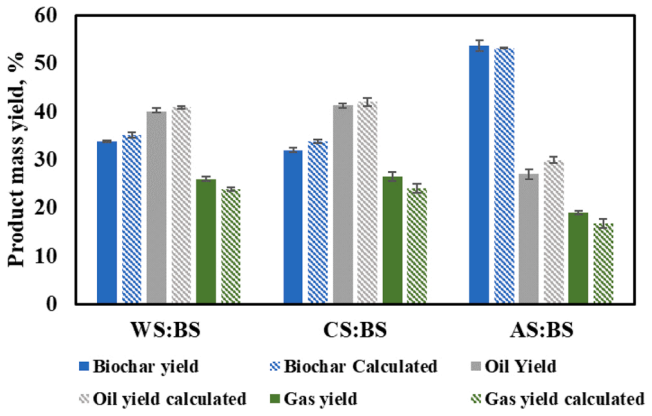

Fig. 2. Comparison of the experimental and calculated product yields of co-pyrolysis (Rathnayake et al., 2022).
AS:BS- Alum sludge and biosolids co-pyrolysis at 3:1, WS:BS- Wheat straw and biosolids co-pyrolysis at 3:1, CS:BS- Canola straw and biosolids co-pyrolysis at 3:1.

feedstocks. Contrary to WS and CS, adding AS increased the biochar and gas yield while decreasing the oil yield compared to the pyrolysis of biosolids. Biochar and oil yield from AS, WS, and CS co-pyrolysis was intermediate to yields from AS, WS and CS, and BS pyrolysis, and this can be explained by the dilution effect of mixing AS and lignocellulosic biomass with BS, which resulted in blends with intermediate levels of ash content. The high gas yield can be explained by minerals in AS and BS promoting tar cracking and secondary reactions that produce non-condensable gases (See Fig. 2) (Zhang et al., 2015a; Choi et al., 2019; Fan et al., 2020). Higher gas yield than both parent feedstock pyrolysis can occur due to interactions between feed materials during co-pyrolysis, known as synergistic effects (Wang et al., 2016b; Jin et al., 2017; Shi et al., 2013).

Synergistic effects between feedstocks in co-pyrolysis refer to the enhanced effects when processed in combination compared to predicted additive effects of individual feedstocks. Therefore, the degree of synergy can be analyzed by the difference between experimental and theoretical values. This study analyzed synergistic effects in product distribution by comparing experimental product yields with calculated product yields, as shown in Fig. 2. Experimental biochar and oil yields were lower than the calculated yield in all co-pyrolysis experiments, while experimental gas yields were higher than the calculated values. These observations indicate the presence of synergistic effects in the co-pyrolysis of biosolids with WS and CS.

However, the mechanism of synergistic effects in different types of co-pyrolysis feedstock may be different. The experimental gas yield was higher than the calculated yield by 4.55% in WS co-pyrolysis and by 4.42% in CS co-pyrolysis (See Fig. 2). Furthermore, the experimental biochar yield was slightly lower than the calculated yield by 0.60% in WS co-pyrolysis and by 0.07% in CS co-pyrolysis (See Fig. 2). The experimental oil yield was lower than the calculated yield by 3.96% in WS co-pyrolysis and by 4.34% in CS co-pyrolysis (See Fig. 2). This result can be explained by the catalytic effects of minerals and metals in biosolids promoting the degradation reactions of volatile organic matter in the feedstock mixtures and intensifying the char cracking reactions, which produce lower molecular weight gaseous products (Wang et al., 2016b; Jin et al., 2017; Zhang et al., 2015a; Yang et al., 2015; Shi et al., 2013). In AS co-pyrolysis, the experimental yield value of oil was much lower than the calculated value (See Fig. 2). The difference between experimental and calculated values was 3.82%.

In contrast, the difference between the calculated and experimental yield values of biochar was insignificant (0.21%). The most significant decrease in oil yield was observed in AS co-pyrolysis. This observation may occur due to increased secondary reactions in co-pyrolysis via mineral components present in biosolids producing low molecular weight gaseous products.

3.2. General properties of biochar

Proximate and ultimate analysis, pH, and higher heating value (HHV) of feedstock and resultant biochar products are presented in Table 1. Images of biochar derived from different experiments can be found in Fig. S3 in the supplementary material. During pyrolysis and co-pyrolysis experiments, volatile matter (VM) content decreased, and ash content increased in all the feedstocks considered. The reason for this phenomenon is the decomposition and conversion of organic matter during thermal treatment (Wang et al., 2016a, 2019, 2020; Huang et al., 2017; Jin et al., 2017). The addition of CS and WS in co-pyrolysis of biosolids experiments led to a significant increase in the VM and a decline in ash and FC content since, compared to biosolids, lignocellulosic biomass (CS and WS) had higher contents of organic matter and lower ash content (Wang et al., 2016a, 2019, 2020; Huang et al., 2017; Jin et al., 2017). When these results were compared to our previous study on AS co-pyrolysis, the addition of AS to BS produced biochar with lower VM and higher ash content compared to BSBC. These results suggest that feedstock composition is a primary factor influencing the proximate composition of derived biochar in both co-pyrolysis and pyrolysis treatments.

C, H, and N content in biochar decreased compared to their feed blend, which is consistent with the literature (Wang et al., 2020, 2022; Huang et al., 2017; Saleh Khodaparasti et al., 2022; Zhang et al., 2020; Ruiz-Gomez et al., 2017). The decrease in C, H, and N occurs due to the decomposition of organic matter during pyrolysis conversion leading to lower C, H, and N contents and higher ash contents (Bai et al., 2021; Huang et al., 2017; Wang et al., 2019; Zhang et al., 2015a). As seen from Table 1, CS: BSBC and WS: BSBC had higher C, H content than BSBC. Due to the increased carbon and hydrogen content and volatile matter, biochar produced from co-pyrolysis of BS and WS compared to BSBC may have applications in agriculture as a soil amendment to treat degraded soil and as a substitute to carbon black in rubber compounding (Peterson, 2022; Sanchez-Reinoso et al., 2020). On the contrary, when this was compared with results from the AS-BS co-pyrolysis study, it could be seen that AS co-pyrolysis biochar (AS: BSBC) had lower C, H content than BS biochar (BSBC). This reduction is due to the high C, H content, and low ash content present in WS and CS compared to BS and AS (See Table 1).

The H/C and O/C ratios decreased in biochar compared to their parent feedstock, the H/C ratio indicates the degree of aromaticity of the biochar, and O/C indicates the polarity of biochar. Lower H/C and O/C ratios imply biochars are more recalcitrant to biological and chemical aging in the environment. This trend agrees with the findings in existing literature, and biochar with lower atomic ratios of H/C and O/C is conducive to C sequestration when incorporated into the soil (Zhang et al., 2015a; Yang et al., 2015). The H/C ratio in biochar derived from co-pyrolysis decreased with the addition of lignocellulosic biomass. However, when this result is compared to AS co-pyrolysis, H/C increases with the addition of AS (Rathnayake et al., 2022).

The higher heating value (HHV) of biochar produced from pyrolysis/co-pyrolysis was lower than the heating value of their parent feedstock. Co-pyrolysis of WS and CS resulted in biochar with improved HHV compared to BSBC, but according to our previous study addition of AS reduced HHV compared to BSBC (Rathnayake et al., 2022). Therefore, biochar produced from co-pyrolysis of biosolids with lignocellulosic biomass is a better option than BSBC in solid fuel applications due to increased calorific value(See Table 1). Meanwhile, biochar from AS co-pyrolysis is suitable as a liming agent due to its high pH value and ash content. Therefore, selecting feedstock for co-pyrolysis based on the intended application of biochar is beneficial.

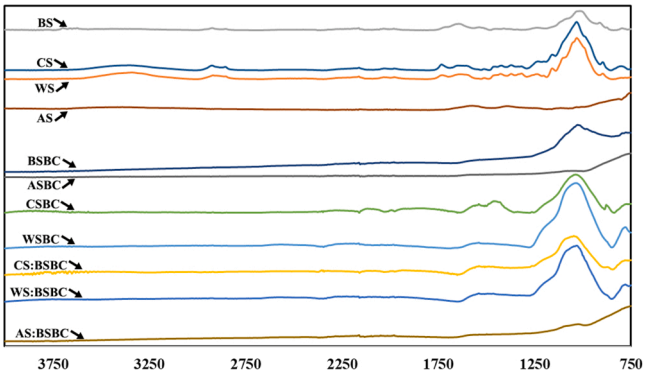

Fig. 3. FTIR spectra of feedstock and biochar prepared from pyrolysis and co-pyrolysis of biosolids with different feedstock (Rathnayake et al., 2022). BS-Biosolids, AS-Alum sludge, WS- Wheat straw, CS- Canola straw, BSBC- Biosolids' biochar, ASBC-Alum sludge biochar, WSBC-Wheat straw biochar, CSBC- Canola straw biochar, AS:BSBC- Biochar derived from alum sludge and biosolids co-pyrolysis at 3:1, WS:BSBC- Biochar derived from wheat straw and biosolids co-pyrolysis at 3:1, CS:BSBC- Biochar derived from canola straw and biosolids co-pyrolysis at 3:1.

3.3. FTIR analysis of biochar

FTIR spectra of raw feedstock and biochar produced from pyrolysis and co-pyrolysis are presented in Fig. 3. Broad peaks with a maximum at 3422 cm^{-1} (OH and NH stretching vibrations), a peak in 2923 cm^{-1} (CH_3 asymmetric stretch vibrations), and bands at 1633 cm^{-1} and 1560 cm^{-1} (presence of amides) and 1035 cm^{-1}(-C═O groups) could be observed in BS, WS and CS FTIR spectra (See Fig. 3) (Patel et al., 2019; Huang et al., 2017; Wang et al., 2019; Yang et al., 2020; Zhang et al., 2015b). In comparison, AS FTIR spectra showed peaks at 1115 cm^{-1} and 794 cm^{-1}, indicating symmetric stretching vibration of Si—O—Si and bending vibration of O—Si—O (See Fig. 3) (Rathnayake et al., 2022; Soleha et al., 2016; Tantawy, 2015). Peaks at 1592 cm^{-1} and 3502 cm^{-1} AS spectra indicated the bending vibration of water that is chemically bonded to Al $(OH)_3$ or OH stretching vibration of $Al(OH)_3$ (See Fig. 3) (Soleha et al., 2016; Tantawy, 2015). The absorption band at 1442 cm^{-1} indicates the presence of carbonate (See Fig. 3) (Soleha et al., 2016; Tantawy, 2015).

O-H peak and the peak corresponding to C-H vibration disappeared and reduced respectively in all biochar (pyrolysis and co-pyrolysis). This trend suggested that large amounts of hydroxyl groups and aliphatic compounds were decomposed in pyrolysis (Patel et al., 2019). However, it can be observed that aromatic C-O stretching (1034 cm^{-1}) and aromatic C = O (794 cm^{-1}) were relatively stable in pyrolysis(See Fig. 3) (Patel et al., 2019). According to Fig. 3, Si—O—Si and carbonate bonds are stable during co-pyrolysis of BS and AS as peaks corresponding to these bonds remained stable from AS spectra to AS: BSBC. However, in CS: BSBC and WS: BSBC, the peak intensity at 1035 cm^{-1} increased compared to BSBC, indicating that during co-pyrolysis, forms of oxygen in the feedstock primarily bonded directly with adjacent carbon atoms, thereby integrating into the carbon chain in the form of carbon-oxygen single bond.

Table 2
BET surface area of feedstocks and biochar produced from pyrolysis/co-pyrolysis of biosolids and alum sludge (Rathnayake et al., 2022).

Biochar sample	BET surface area (m^2/g)
BS	3.06 ± 0.16
WS	2.50 ± 1.41
CS	4.07 ± 1.96
BSBC	89.32 ± 1.11
WSBC	119.36 ± 3.71
CSBC	101.61 ± 3.69
WS:BSBC	83.61 ± 3.11
CS:BSBC	74.68 ± 5.89
AS	7.95 ± 1.38
ASBC	35.18 ± 2.19
AS:BSBC	24.52 ± 0.91

BS-Biosolids, AS-Alum sludge, WS- Wheat straw, CS- Canola straw, BSBC- Biosolids' biochar, ASBC-Alum sludge biochar, WSBC-Wheat straw biochar, CSBC- Canola straw biochar, AS:BSBC- Biochar derived from alum sludge and biosolids co-pyrolysis at 3:1, WS:BSBC- Biochar derived from wheat straw and biosolids co-pyrolysis at 3:1, CS:BSBC- Biochar derived from canola straw and biosolids co-pyrolysis at 3:1

3.4. Surface morphology of biochar

The BET surface areas of feedstock and biochar are presented in Table 2. It can be seen that biochar derived from both pyrolysis and co-pyrolysis had improved surface area compared to the feedstock. The highest increase in surface area was reported in WS, followed by CS, while biosolids reported the lowest increase in surface area during pyrolysis. The high volatile matter content can explain this observation in WS and CS compared to BS. The release of this volatile content during pyrolysis created more pores, thus increasing surface area. This theory can be further confirmed since the highest reduction of VM was reported in WS pyrolysis, from 74.04% to 30.58%.

The surface area reported in our previous study for co-pyrolysis biochar with AS was lower than CS: BSBC and WS: BSBC, where BET surface area was reduced by 24.5% compared to BSBC (See Table 2) (Rathnayake et al., 2022). This decrease can be attributed to the lower volatile matter present in AS compared to biosolids (Choi et al., 2019; Dassanayake et al., 2015). However, the surface area of CS: BSBC and WS: BSBC also were slightly lower than BSBC, which can be explained by tar produced in the co-pyrolysis process adhering to the biochar surface, resulting in blockage of the porous structure (Wang et al., 2020; Huang et al., 2017; Jin et al., 2017).

SEM images of the biochar from different feedstock are shown in Fig. 4. It is visible that biosolids' biochar (BSBC) has a porous and well-defined crystalline structure (See Fig. 4(a)). Fig. 4(e) shows that the addition of alum sludge does not have a visible effect on biosolids' biochar particles in AS: BS BC. However, from the SEM images from co-pyrolysis of biosolids with WS and CS (See Figs. 4(f) and 4(g)), it can be seen that there are some blockages in the pores, which can be due to tar adhering to biosolids' biochar as previously explained (Wang et al., 2020; Huang et al., 2017; Jin et al., 2017). Despite the tar depositions, this biochar can still be used in agricultural applications or as a substitute for carbon black in rubber compounding (Peterson, 2022; Sanchez-Reinoso et al., 2020). However, tar depositions on the biochar intended to be applied as adsorbents can be removed, and surface area can be increased by exposing the biochar to steam or CO_2 at high temperatures (Feng et al., 2018; Geca et al., 2022).

3.5. Total Heavy metal concentration in biochar

The total concentrations of As, Cd, Cr, Cu, Ni, Pb, Se, and Zn present in the feed materials and the resultant biochar are presented in Table 3. Heavy metal concentrations for AS pyrolysis and co-pyrolysis obtained from our previous study are also included in Table 3 (Rathnayake et al., 2022). High heavy metal concentration is the main limitation of land application of biosolids and biosolids' biochars. Heavy metal contamination in agricultural land may lead to contamination in the food chain, causing severe health problems in human beings. EPA Victorian Biosolids Guidelines ensure biosolids' safe handling and reuse to protect human and animal health, the environment, and agricultural products in Victoria, Australia (Irwin et al., 2017). In EPA Guidelines, biosolids are classified into two primary contamination grades based on their total heavy metal concentration (Irwin et al., 2017). Biosolids categorized as Grade C1 have the lowest concentration of heavy metals, and they can

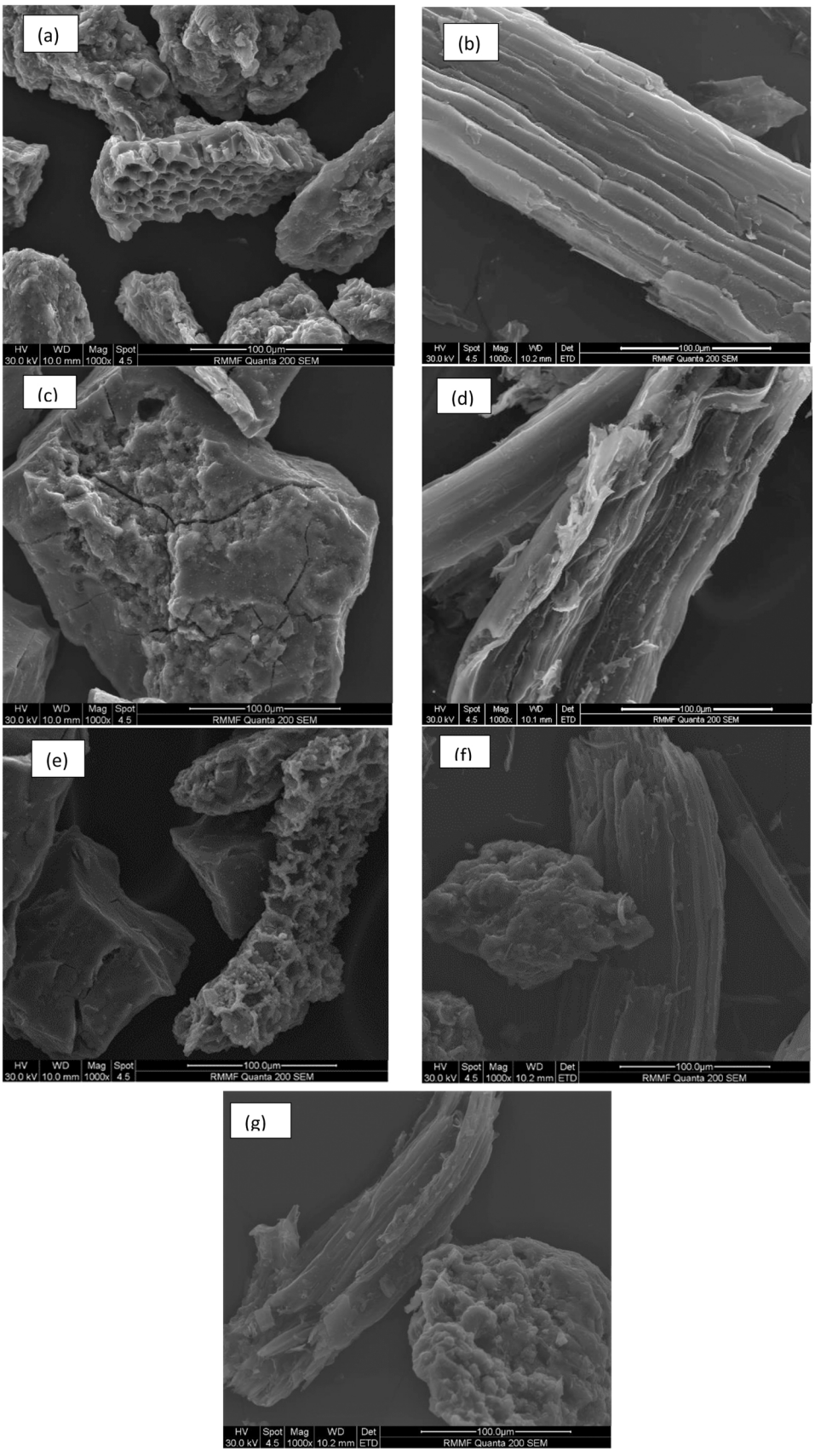

Fig. 4. SEM micrograph of (a) BSBC, (b) WSBC, (c) ASBC, (d) CSBC (e) AS:BS BC, (f) WS:BS BC, (g) CS:BSBC (Rathnayake et al., 2022).
BS-Biosolids, AS-Alum sludge, WS- Wheat straw, CS- Canola straw, BSBC- Biosolids' biochar, ASBC-Alum sludge biochar, WSBC-Wheat straw biochar, CSBC- Canola straw biochar, AS:BSBC- Biochar derived from alum sludge and biosolids co-pyrolysis at 3:1, WS:BSBC- Biochar derived from wheat straw and biosolids co-pyrolysis at 3:1, CS:BSBC- Biochar derived from canola straw and biosolids co-pyrolysis at 3:1.

Table 3
Heavy metal concentration (mg/kg) in feedstocks and resultant biochar from pyrolysis and co-pyrolysis experiments and contaminant upper limits for classifying biosolids grade C1 and C2 according to EPA Victoria Biosolids Guidelines (Rathnayake et al., 2022; Irwin et al., 2017).

Heavy metals	Feedstocks (mg/kg)			Pyrolysis biochar (mg/kg)			Co-pyrolysis biochar (mg/kg)		AS co-pyrolysis data (mg/kg)			C1 Grade (mg/kg)	C2 Grade (mg/kg)
	BS	WS	CS	BSBC	WSBC	CSBC	WS: BSBC	CS: BSBC	AS	ASBC	AS: BS BC		
As	4.63 ± 0.185	< 0.1	< 0.1	3.84 ± 1.17	< 0.1	< 0.1	< 0.1	< 0.1	9.91 ± 0.05	12.52 ± 1.72	3.09 ± 1.42	20	60
C d	1.10 ± 0.46	< 0.1	1.05 ± 0.12	1.5 ± 0.09	< 0.1	< 0.1	< 0.1	< 0.1	< 0.1	0.21 ± 0.03	0.5 ± 0.03	1	10
Cr	21.03 ± 2.48	3.11 ± 1.01	3.59 ± 0.43	55.56 ± 2.22	11.09 ± 4.34	11.87 ± 0.64	23.89 ± 2.31	24.54 ± 2.15	4.03 ± 1.49	11.65 ± 1.18	15.91 ± 3.05	400	3000
Cu	1014.41 ± 2.21	2.62 ± 0.94	8.90 ± 2.44	1998.47 ± 149.24	9.24 ± 2.82	26.70 ± 5.65	768.24 ± 32.67	734.30 ± 54.43	79.35 ± 2.83	119.78 ± 1.89	412.99 ± 13.51	100	2000
Ni	8.83 ± 1.59	1.68 ± 0.88	2.11 ± 0.99	42.01 ± 3.99	6.04 ± 1.43	6.86 ± 2.43	14.87 ± 5.11	16.08 ± 3.11	12.12 ± 2.06	26.18 ± 1.91	43.06 ± 1.53	60	270
Pb	23.03 ± 2.02	2.32 ± 1.21	2.66 ± 0.23	51.52 ± 1.53	7.34 ± 2.11	8.79 ± 1.54	23.25 ± 8.64	25.98 ± 5.13	0.97 ± 0.935	2.04 ± 0.98	13.77 ± 2.65	300	500
Se	4.52 ± 0.30	< 1	< 1	5.51 ± 1.2	< 1	< 1	< 1	< 1	< 1	< 1	< 1	3	50
Zn	895.44 ± 32.28	26.73 ± 1.55	18.67 ± 0.89	2230.16 ± 134.92	107.12 ± 2.11	61.67 ± 4.41	748.43 ± 32.65	794.14 ± 28.70	60.77 ± 9.62	145.31 ± 35.43	453.31 ± 3.35	200	2500

BS-Biosolids, AS-Alum sludge, WS- Wheat straw, CS- Canola straw, BSBC- Biosolids' biochar, ASBC-Alum sludge biochar, WSBC-Wheat straw biochar, CSBC- Canola straw biochar, AS:BSBC- Biochar derived from alum sludge and biosolids co-pyrolysis at 3:1, WS:BSBC- Biochar derived from wheat straw and biosolids co-pyrolysis at 3:1, CS:BSBC- Biochar derived from canola straw and biosolids co-pyrolysis at 3:1

be used in unrestricted land applications (Irwin et al., 2017). The highest allowable limits of heavy metal concentrations in BS to be fit for unrestricted land applications according to the EPA Victorian Biosolids Guidelines are shown in Table 3 (Irwin et al., 2017).

In the Victorian biosolids samples used in the current study, Cu, Zn, Cd, and Se concentrations were above the allowable limits to be classified as C1 (Irwin et al., 2017). It can be seen from Table 3 that WS and CS have substantially lower heavy metal content compared to biosolids.

Heavy metal concentrations in biochar products derived from pyrolysis experiments were higher compared to their parent feed material. This result can be explained by the higher thermal stability of heavy metals compared to the other organic components present in the feed sample (Yang et al., 2018; Wang et al., 2019; Jin et al., 2017; Ruiz-Gomez et al., 2017). Therefore, BSBC had higher Cu, Se, and Zn concentrations than BS; however, they were still within limits for C2 grade (Agency, 2021). Heavy metal was enriched by a factor of 2.1–3 in WS and CS pyrolysis, higher than AS co-pyrolysis (See Table 3) (Rathnayake et al., 2022). According to our previous study, AS co-pyrolysis reported that heavy metal in AS biochar (ASBC) was enriched by a factor of 0.26–2.68 compared to AS (See Table 3) (Rathnayake et al., 2022). This difference can be attributed to the high yield of biochar obtained in AS: BS co-pyrolysis compared to WS and CS (Rathnayake et al., 2022).

As expected, biochar produced from co-pyrolysis experiments had significantly lower concentrations of Cd, Cr, Cu, Pb, Se, and Zn than BSBC (See Table 3). Cd and Se concentrations in biochar co-pyrolysis biochar were sufficiently lower to be within the limits of Grade C1. However, Cu and Zn concentrations WS: BSBC and CS: BSBC still exceeded the limits to be classified as Grade C1, but their concentrations were significantly lower than BSBC. Cu concentration was reduced by 61.55% and 58.25%, and Zn concentration was reduced by 66.44% and 64.39% in WS: BSBC and CS: BSBC, respectively (See Table 3). Therefore biochar produced from co-pyrolysis of biosolids with AS, WS, and CS will be more beneficial in agricultural applications than BSBC due to significantly lower heavy metal concentrations in AS: BS BC, WS: BS BC, and CS: BS BC (Peterson, 2022; Sanchez-Reinoso et al., 2020). The dilution effect can explain this reduction of heavy metal concentration in co-pyrolysis biochar due to blending biosolids with feeds with considerably lower concentrations of heavy metals. It was also observed that synergistic effects in co-pyrolysis also impacted the heavy metal content in co-pyrolysis biochar. Fig. 5 compares experimental and calculated heavy metal concentrations in co-pyrolysis biochar. The calculated value of heavy metal concentration was obtained by assuming the synergistic effect is non-existent and co-pyrolysis biochar

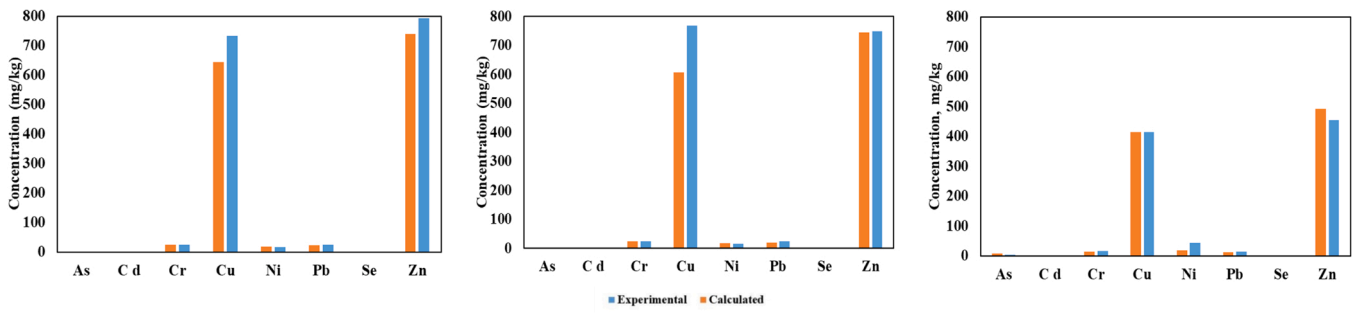

Fig. 5. Comparison of experimental and calculated heavy metal concentration in co-pyrolysis biochar (a) CS:BS BC, (f) WS:BS BC, (g) AS:BS BC (Ischia et al., 2011).

was simply a mixture of BSBC and CSBC, WSBC, or ASBC. However, it can be seen in CS: BSBC and WS: BSBC that experimental heavy metal concentration is higher than the calculated values (especially Cu and Zn). This phenomenon can be explained by the synergistic effect in CS and WS co-pyrolysis reducing the biochar yield, as explained previously in the product yield section, which leads to higher heavy metal concentration in their resultant biochars. However, according to our previous study, this trend was not observed in AS co-pyrolysis (Rathnayake et al., 2022; Adapa and Schoenau, 2009). Furthermore, in AS co-pyrolysis, the experimental Zn concentration was lower than the calculated value, which can be due to the higher concentration of Cl present in AS leading to the formation of $ZnCl_2$ (Rathnayake et al., 2022; Choi et al., 2019; Johansen et al., 2011).

The total metal contents in biochars may not accurately represent the risk of plant uptake. Several studies reported that during thermochemical conversion processes, heavy metal components present in the feed materials convert into more stable fractions (Yang et al., 2018; Wang et al., 2020, 2019). The DTPA (diethylenetriaminepentaacetic acid) extraction method is a non-equilibrium extraction method used for estimating the soil availability of heavy metals. Previous studies have found that this method correlates well with the crop response (Yang et al., 2018; Mühlbachová, 2002). Therefore, the current study used the DTPA extraction method to estimate the potential plant-available heavy metals. Table 4 includes feedstock's DTPA-extractable heavy metal concentrations (Cd, Cu, Ni, Pb, and Zn) and their resultant biochar. As expected, DTPA-extractable concentrations of the considered heavy metals in biochar were significantly lower than their raw material, and it is consistent with the previous studies (Patel et al., 2019; Zhang et al., 2020). This observation indicates that co-pyrolysis significantly reduced the extractable heavy metal concentrations. This decrease in plant-available heavy metal concentration can be explained by the development of functional groups on biochar surfaces. These developed functional groups resulted in the immobilization of heavy metals by forming organic-metallic complexes (Patel et al., 2019; Zhang et al., 2020). WS: BSBC and CS: BSBC showed a higher difference between total and DTPA extractable heavy metal concentrations of Cu, Ni, and Zn than AS co-pyrolysis biochar (Rathnayake et al., 2022). Nevertheless, biochar derived from the co-pyrolysis of biosolids had only very low concentrations of plant-available heavy metals.

3.6. Pyrolysis/ Co-pyrolysis oil characterization

Oil derived from pyrolysis and co-pyrolysis experiments are complicated mixtures of a large number of organic compounds. These organic compounds and their concentration in oil varies from feedstock to feedstock. Therefore, different shades of dark brown in the oil samples, as shown in Fig. S4, may attribute to their composition. The composition of oil produced from each experiment was determined by identifying more than 70 compounds using GC-MS analysis, and these compounds are listed in supplementary data (Table S1). These compounds were categorized into aliphatic, aromatic, nitrogenated, oxygenated, and polyaromatic compounds (PAC) based on several previous studies in the literature (Patel et al., 2019; Fonts et al., 2009; Jindarom et al., 2007).

Fig. 6 illustrates the distribution of oil compounds from pyrolysis/co-pyrolysis of biosolids with AS, WS, and CS. In the current study, AS pyrolysis and co-pyrolysis oil data from our previous study were compared with WS and CS pyrolysis and co-pyrolysis oil data (Rathnayake et al., 2022). The aromatics group comprised the highest proportion of all the pyrolysis and co-pyrolysis oils, consisting of benzene and its derivatives, phenols, phenol derivatives, and furans. The presence of these compounds in oils is desirable as they have various applications in chemical industries, especially as solvents (Patel et al., 2019; Fonts et al., 2009; Jindarom et al., 2007). Pyrolysis oil produced from WS and CS had a comparatively higher amount of aromatic compounds than BS pyrolysis oil. The high composition of aromatic compounds in WS and CS pyrolysis oil can be attributed to the thermal degradation of lignin, which is high in WS and CS (Wang et al., 2016a; Alvarez et al., 2015). It can be seen that the proportion of aromatics in co-pyrolysis oil was higher than in the individual feedstock pyrolysis oils, which may occur due to the catalytic effect of ash content in biosolids promoting aromatization reactions (Alvarez et al., 2015).

A substantial amount of nitrogenated compounds were observed in biosolids and AS pyrolysis and co-pyrolysis oils, which comprise amines and amides such as pyridine, pyrazole, and imidazole. The high amount of nitrogenated components in oil significantly limits its application as a liquid fuel due to its detrimental effects, such as gum or heavier product formation, inhibition and deactivation of an acid catalyst, acid−base pair-related corrosion, and metal complexation (Patel et al., 2019; Alvarez et al., 2015; Zhang et al., 2015a; Zuo et al., 2014). It can be observed that the addition of WS and CS significantly reduced these undesirable nitrogenated compounds. Compounds such as naphthalene and indene constitute the PACs group which is also highly undesirable (Patel et al., 2019). However, PACs were only present in a small proportion of AS co-pyrolysis oil and were negligible in co-pyrolysis oil from WS and CS.

Oxygenated compounds include aldehydes, ketones, esters, and carboxylic acids (Patel et al., 2019; Rathnayake et al., 2022). WS and CS pyrolysis oils contained a high proportion of oxygenated compounds at 48.17% and 52.34%, respectively (See Fig. 6). These compounds in lignocellulosic feedstock were produced from the decomposition of hemicellulose, cellulose, and lignin (Patel et al., 2019; Wang et al., 2016a; Lan et al., 2020; Vasu et al., 2019). Oxygenated compounds in co-pyrolysis oil were reduced to 19.3% and 29.9% WS: BS oil and CS: BS oil, respectively (See Fig. 6). This decrease may occur due to the intensification of de-nitrification and deoxygenation reactions of long

Table 4
DTPA extracted heavy metal concentration (mg/kg) in feedstock and resultant biochar from pyrolysis and co-pyrolysis experiments (Rathnayake et al., 2022).

Heavy metals	Feedstocks			Pyrolysis biochar			Co-pyrolysis biochar		AS co-pyrolysis data		
	BS	WS	CS	BSBC	WSBC	CSBC	WS: BSBC	CS: BSBC	AS	ASBC	AS: BSBC
Cd	0.60 ± 0.36	< 0.01	< 0.01	< 0.01	< 0.01	< 0.01	< 0.01	< 0.01	< 0.01	< 0.01	< 0.01
Cu	332.85 ± 80.13	< 1	< 1	29.87 ± 9.51	0.42 ± 0.27	0.31 ± 0.11	1.12 ± 0.98	1.32 ± 0.87	0.81 ± 0.32	0.71 ± 0.27	3.71 ± 0.83
Ni	5.47 ± 0.97	< 1	< 1	0.08 ± 0.21	0.07 ± 0.05	0.08 ± 0.24	0.04 ± 0.02	0.012 ± 0.007	0.70 ± 0.51	0.06 ± 0.26	0.008 ± 0.005
Pb	1.14 ± 0.72	0.54 ± 0.23	0.43 ± 0.22	0.34 ± 0.97	0.06 ± 0.34	0.03 ± 0.11	0.32 ± 021	0.43 ± 0.21	0.25 ± 0.76	0.01 ± 0.18	0.22 ± 0.36
Zn	404.37 ± 36.76	1.03 ± 0.77	0.86 ± 0.12	32.65 ± 8.43	0.11 ± 0.08	0.099 ± 0.07	10.32 ± 3.11	11.46 ± 3.10	2.13 ± 0.83	0.16 ± 0.08	9.55 ± 0.75

BS-Biosolids, AS-Alum sludge, WS- Wheat straw, CS- Canola straw, BSBC- Biosolids' biochar, ASBC-Alum sludge biochar, WSBC-Wheat straw biochar, CSBC- Canola straw biochar, AS:BSBC- Biochar derived from alum sludge and biosolids co-pyrolysis at 3:1, WS:BSBC- Biochar derived from wheat straw and biosolids co-pyrolysis at 3:1, CS:BSBC- Biochar derived from canola straw and biosolids co-pyrolysis at 3:1

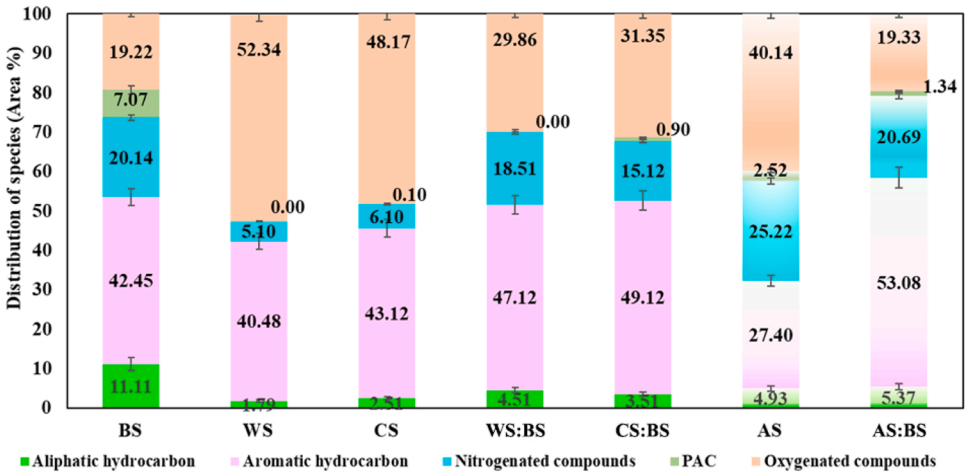

Fig. 6. Composition of pyrolysis/co-pyrolysis oil produced from different feedstock (Rathnayake et al., 2022).
BS- Biosolids pyrolysis oil, AS-Alum sludge pyrolysis oil, WS- Wheat straw pyrolysis oil, CS- Canola straw pyrolysis oil, AS:BS- Oil derived from alum sludge and biosolids co-pyrolysis at 3:1, WS:BS- Oil derived from wheat straw and biosolids co-pyrolysis at 3:1, CS:BS- Oil derived from canola straw and biosolids co-pyrolysis at 3:1.

straight-chain compounds. The minerals present in feedstocks during co-pyrolysis lead to the production of incondensable hydrocarbons, which is consistent with the high experimental gas yield in Fig. 2 (Jin et al., 2017; Lan et al., 2020; Zhang et al., 2015a; Zhu et al., 2018; Park et al., 2019). High oxygenated compounds in co-pyrolysis oil products hinder oil's miscibility with hydrocarbon fuels, undergo phase separation during storage, and may also cause instability of oil over time (Abdul Rahman Mohamed, 2020). Thus, these oil products have little potential to replace conventional fossil fuels (Abdul Rahman Mohamed, 2020). However, this oil may be used in commercial pyrolysis or co-pyrolysis reactor to achieve energy self-sufficiency by combusting produced oil products in a downstream stem to provide the heat energy required for thermal decomposition reactions. Alkanes, alkenes, and their derivatives are categorized as aliphatic hydrocarbons. A high amount of aliphatic compounds can be observed in oil derived from biosolids pyrolysis due to the high mineral content in biosolids ash, which promotes cracking reactions of high molecular weight compounds (Patel et al., 2019; Wang et al., 2016a; Lan et al., 2020; Vasu et al., 2019).

pH values of the extracted oil samples, shown in Fig. 7, were analyzed to study the fuel acidity and corrosiveness. The addition of WS and CS decreased the pH value to 4.3 and 3.9, respectively (See Fig. 7). The high acidity of co-pyrolysis oil produced from WS and CS can be attributed to the presence of organic acids from the degradation of cellulose and hemicellulose from WS and CS (Vasu et al., 2019). When these results were compared to AS co-pyrolysis, the oil produced in that scenario was highly basic (9.5) (Rathnayake et al., 2022). The high basicity of these pyrolysis and co-pyrolysis oil produced from BS and AS could be due to the presence of ammonia and nitrogenated protein-derived compounds (Choi et al., 2019; Vasu et al., 2019).

3.7. Pyrolysis/ Co-pyrolysis gas characterization

The molar compositions of CO_2, CO, H_2, CH_4, ethane, and propane in the exhaust gas stream from the reactor are shown in Fig. 8. In each experiment, exhaust gas stream samples were extracted and analyzed every 4 min from the time furnace was turned on to the completion of the experiment. In the first 20 min, the reactor was heated to pyrolysis temperature, and the temperature was maintained for the next 60 min. The concentration of pyrolysis gases increased in the 0–30 min period due to further bond breaking and the release of volatile gases with increasing temperature and then gradually decreased with time due to a shortage of remaining volatile matter (See Fig. 8) (He et al., 2018).

The gas evolution pattern varied with the feedstock. In biosolids pyrolysis, H_2 was the dominant component. WS and CS pyrolysis primarily produced CO, followed by H_2 and methane, and both feedstocks had similar gas evolution patterns (See Fig. 8). The most notable difference between WS and CS gas evolution is that CS produced a higher percentage of co-pyrolysis gases (CO, H_2, CH_4, ethane, and propane). Production of these gases is favored because of their energy value. CO and CO_2 are produced by rearranging the unstable structures of cellulose and hemicellulose (He et al., 2018). Therefore, the notable higher concentration of CO in CS pyrolysis than in WS can be attributed to higher cellulose and hemicellulose content in CS (Svärd, 2018; Tufail et al., 2018).

The exhaust gas stream from co-pyrolysis of BS with WS and CS produced a significantly higher proportion of CO, H_2, CH_4, ethane, and propane than BS pyrolysis (See Fig. 8). In co-pyrolysis experiments maximum evolution of H_2, CO_2, and CH_4 gases shifted to a later period at 30–60 min, compared to pyrolysis experiments (See Fig. 8). Similar to pyrolysis of WS and CS, co-pyrolysis of CS produced higher proportions of co-pyrolysis gases than WS.

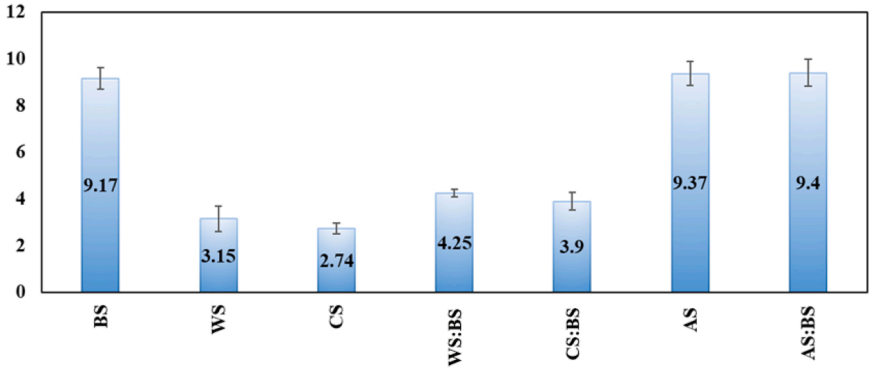

Fig. 7. pH values of pyrolysis/co-pyrolysis oil produced from different feedstocks (Rathnayake et al., 2022).
BS- Biosolids pyrolysis oil, AS-Alum sludge pyrolysis oil, WS- Wheat straw pyrolysis oil, CS- Canola straw pyrolysis oil, AS:BS- Oil derived from alum sludge and biosolids co-pyrolysis at 3:1, WS:BS- Oil derived from wheat straw and biosolids co-pyrolysis at 3:1, CS:BS- Oil derived from canola straw and biosolids co-pyrolysis at 3:1.

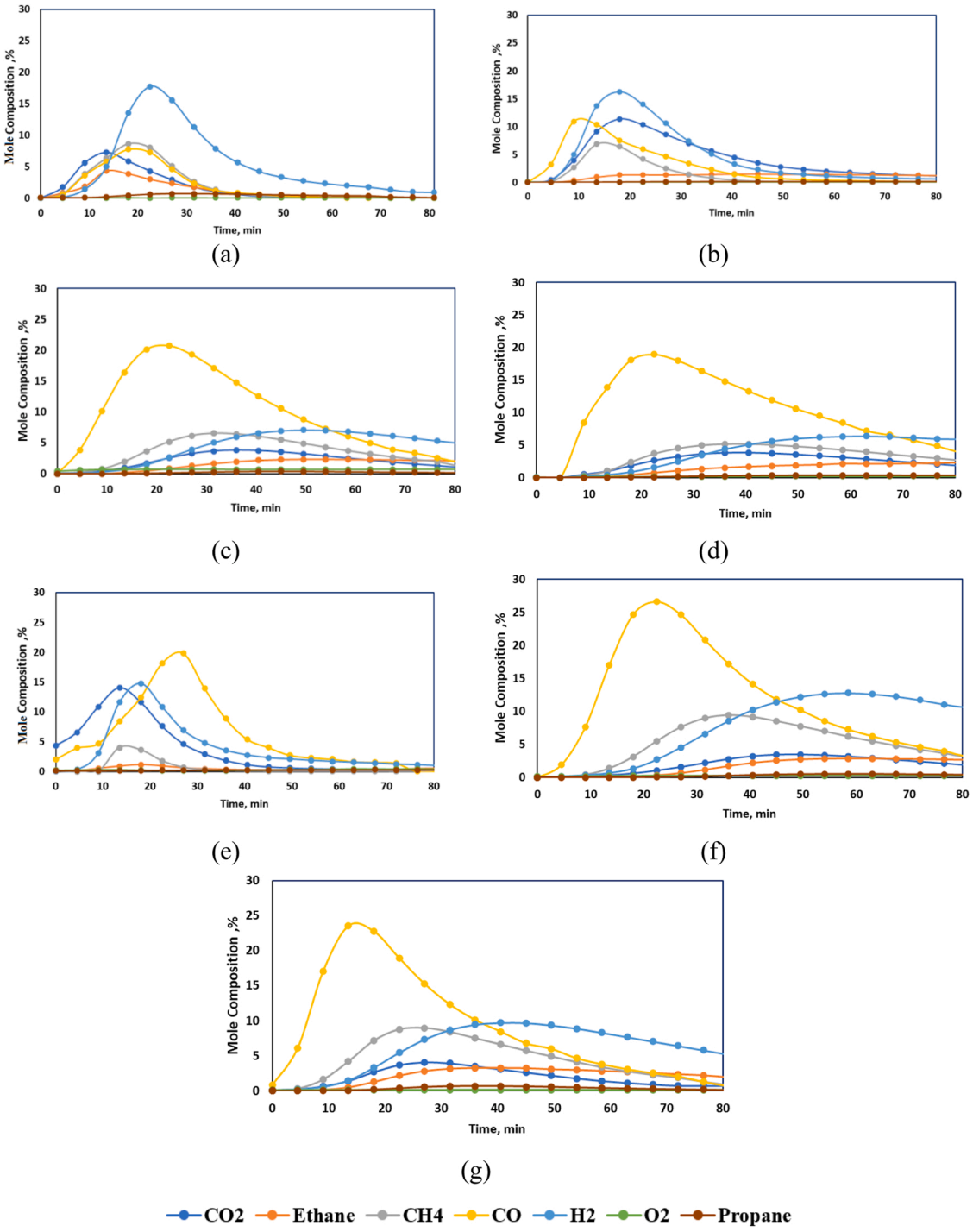

Fig. 8. Gas product composition of pyrolysis and co-pyrolysis of (a) BS GP, (b) AS GP, (c) CS GP, (d) WS GP, (e) AS: BSGP, (f) CS: BS GP, (g) WS: BS GP (Rathnayake et al., 2022).
BS GP-Biosolids pyrolysis gas product, AS GP -Alum sludge pyrolysis gas product, WS GP - Wheat straw pyrolysis gas product, CS GP- Canola straw pyrolysis gas product, AS:BS GP- Gas product derived from alum sludge and biosolids co-pyrolysis at 3:1, WS:BS GP- Gas product derived from wheat straw and biosolids co-pyrolysis at 3:1, CS:BS GP- Gas product derived from canola straw and biosolids co-pyrolysis at 3:1.

Furthermore, these results were compared with our previous study on the co-pyrolysis of biosolids with AS (Rathnayake et al., 2022). AS pyrolysis produced H_2 as the dominant compound, and higher concentrations of CO_2 and CO compared to BS pyrolysis were also observed(See Fig. 8) (Rathnayake et al., 2022). Co-pyrolysis gas proportion in the outlet stream was significantly lower in AS: BS co-pyrolysis compared to WS: BS and CS: BS, which can be due to the higher amount of volatile matter present in CS and WS (He et al., 2018). Also, these lignocellulosic biomasses are mainly composed of C, H, O, and other elements, which can be converted into non-condensable gases during co-pyrolysis (He et al., 2018).

The mole composition of gas produced from the co-pyrolysis of biosolids indicated apparent synergistic effects, especially in H_2 and CO compositions (See Fig. 8) (Rathnayake et al., 2022). These synergistic effects can occur due to minerals in biosolids intensifying tar decomposition resulting in lighter molecular weight components such as H_2

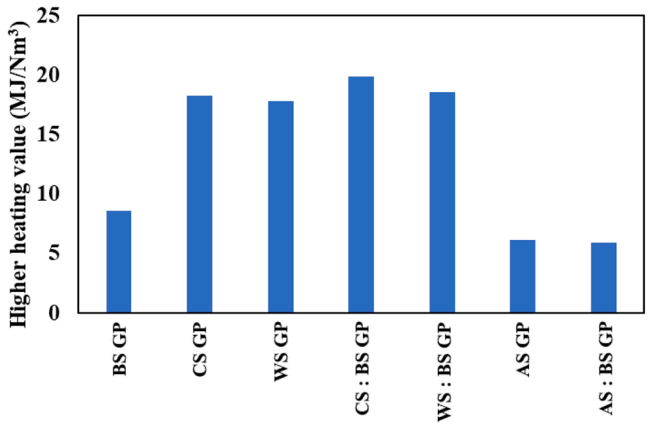

Fig. 9. Higher heating values of the gas produced from pyrolysis and co-pyrolysis experiments (Rathnayake et al., 2022).
BS GP-Biosolids pyrolysis gas product, AS GP -Alum sludge pyrolysis gas product, WS GP - Wheat straw pyrolysis gas product, CS GP- Canola straw pyrolysis gas product, AS:BS GP- Gas product derived from alum sludge and biosolids co-pyrolysis at 3:1, WS:BS GP- Gas product derived from wheat straw and biosolids co-pyrolysis at 3:1, CS:BS GP- Gas product derived from canola straw and biosolids co-pyrolysis at 3:1.

and CO, or that bound water and AAEM provided by biosolids facilitated and intensified H_2O- char gasification and CO_2 gasification (Zhang et al., 2015a; Zhu et al., 2018; Yang et al., 2015). WS and CS co-pyrolysis gas evolution patterns were similar, and in AS co-pyrolysis, gas evolution was different, but CO was the dominant component in all co-pyrolysis experiments. The highest proportion of CO and CH_4 was observed in WS: BS co-pyrolysis, followed by CS: BS, and in AS: BS co-pyrolysis, the CO proportion was significantly lower. This difference can be due to higher C and H content in WS and CS.

The heating values of gases produced from pyrolysis and co-pyrolysis experiments are shown in Fig. 9. The molar composition of gas components was calculated by integrating the gas evolution graphs obtained by micro-GC analysis, and higher heating value (HHV) was calculated by Eq. 5. As shown in Fig. 9, CS and WS gas products had higher HHV than BS and AS, which can be attributed to lower CO concentration in BS and AS gas products, and it can be explained by lower C content present in the BS and AS feedstocks. Co-pyrolysis gas products from WS: BS and CS: BS co-pyrolysis had higher HHV than their parent feedstocks' gas products from pyrolysis. This result shows the beneficial synergistic effects of co-pyrolysis of biosolids with lignocellulosic biomass, and it can be attributed to the higher ethane, propane, methane, and H_2 composition in co-pyrolysis gas products. These results are consistent with our earlier hypothesis that alkali metals in biosolids promote char cracking reactions, leading to increased production of low molecular weight gas products such as ethane, propane, methane, and H_2 (Wang et al., 2016b; Jin et al., 2017; Zhang et al., 2015a; Yang et al., 2015; Shi et al., 2013). However, the HHV of AS: BS gas was lower than both BS gas and AS gas. This phenomenon is consistent with the earlier observation of higher CO_2 concentration and lower CH_4 concentration in AS: BS gas.

4. Conclusions

- Feedstock type and composition significantly affect the co-pyrolysis of biosolids product yields and their properties, and suitable feedstock to perform co-pyrolysis with biosolids must be selected based on the intended applications of the products.
- The addition of lignocellulosic biomass produced biochar with higher C and H content, aromaticity, and calorific value, which will be beneficial for treating degraded soil.
- Co-pyrolysis biochar, oil, and gas product yields also depended on the ash content and volatile matter in the parent feedstocks.
- Heavy metal concentrations in co-pyrolysis biochars were notably lower compared to BSBC.
- According to BET analysis and SEM imaging, the addition of WS and CS resulted in slightly lower surface areas due to tar deposition in biochar particles leading to blocked pores in biosolids' biochar.
- The addition of WS and CS improved oil quality by reducing nitrogenated compounds and eliminating undesirable PAC compounds. However, the addition of lignocellulosic biomass increased the acidity of co-pyrolysis oil.
- The composition of pyrolysis gas from co-pyrolysis of biosolids showed synergistic effects, especially in H_2 and CO gas concentrations. However, the interactions between feedstocks were different in lignocellulosic biomass and biosolids compared to AS and biosolids, which needs further investigation.

Declaration of Competing Interest

The authors declare that they have no known competing financial interests or personal relationships that could have appeared to influence the work reported in this paper.

Acknowledgments

The authors wish to acknowledge RMIT University, Australia, South East Water, Melbourne Water, Intelligent Water Networks (IWN), and ARC Training Centre for Transformation of Australia's Biosolids Resource for the postgraduate scholarships and the financial assistance provided.

Appendix A. Supporting information

Supplementary data associated with this article can be found in the online version at doi:10.1016/j.psep.2023.02.087.

References

Abdul Rahman Mohamed, M.M., Upgrading pyrolysis-derived bio-oils via catalytic hydrodeoxygenation: an overview of advanced nanocatalysts, in New Dimensions in Production and Utilization of Hydrogen. 2020. p. 241–272.
Abnisa, F., Wan Daud, W.M.A., 2014. A review on co-pyrolysis of biomass: An optional technique to obtain a high-grade pyrolysis oil. Energy Convers. Manag. 87, 71–85.
Adapa, P., Schoenau, L.T., G., 2009. Compaction characteristics of barley, canola, oat and wheat straw. Biosyst. Eng. 104, 335–344.
Adapa, P., Tabil, L., Schoenau, G., 2009. Compaction characteristics of barley, canola, oat and wheat straw. Biosyst. Eng. 104 (3), 335–344.
Agency, U.S.E.P.. Land Application of Biosolids. Biosolids 2021 19/02/2021 6/06/2021]; Available from: https://www.epa.gov/biosolids/land-application-biosolids.
Alen Horvat, M.K. and J.J.L., Tar from pilot scale co-pyrolysis of biological dairy sludge and spruce wood chips. Energy Procedia, 2019. 161: p. 66–74.
Ali, L., et al., 2022. Characteristics of biochars derived from the pyrolysis and co-pyrolysis of rubberwood sawdust and sewage sludge for further applications. Sustainability 14, 7.
Alvarez, J., et al., 2015. Fast co-pyrolysis of sewage sludge and lignocellulosic biomass in a conical spouted bed reactor. Fuel 159, 810–818.
André R. Fajardo, A.G.B.Pa.E.C.M., Hydrogels Nanocomposites Based on Crystals, Whiskers and Fibrils Derived from Biopolymers. Eco-friendly Polymer Nanocomposites, 2015. 74.
Bai, J., et al., 2021. Co-pyrolysis of sewage sludge and pinewood sawdust: the synergistic effect and bio-oil characteristics. Biomass Convers. Biorefin.
Batista, R.R., Gomes, M.M., 2021. Effects of chemical composition and pyrolysis process variables on biochar yields: correlation and principal component analysis. Floresta e Ambient. 28, 3.
Choi, D., et al., 2019. Valorization of alum sludge via a pyrolysis platform using CO_2 as reactive gas medium. Environ. Int. 132, 105037.
Dassanayake, K.B., et al., 2015. A review on alum sludge reuse with special reference to agricultural applications and future challenges. Waste Manag. 38, 321–335.
Department of Agriculture, W.a.t.E. Australian Agricultural Census 2015–16 visualisations. 2019; Available from: https://www.awe.gov.au/abares/data/agricultural-census-visualisations.
Department of Economic Development, J., Transport and Resources, Grains industry profile. 2014, State Governement Victoria: Victoria.
Dong, Q., et al., 2019. Co-pyrolysis of sewage sludge and rice straw: thermal behavior and char characteristic evaluations. Energy Fuels 34 (1), 607–615.

Fadhilah, N.A., M.N. Islam, and R. Rosli, Product distribution in fluidized bed co-pyrolysis of sawdust and rice husk, in 8th Brunei International Conference on Engineering and Technology 2021. 2023.
Fan, S., et al., 2016. Biochar prepared from co-pyrolysis of municipal sewage sludge and tea waste for the adsorption of methylene blue from aqueous solutions: Kinetics, isotherm, thermodynamic and mechanism. J. Mol. Liq. 220, 432–441.
Fan, Y., et al., 2020. Minimizing tar formation whilst enhancing syngas production by integrating biomass torrefaction pretreatment with chemical looping gasification. Appl. Energy **260**.
Fei, J., et al., 2012. Synergistic effects on co-pyrolysis of lignite and high-sulfur swelling coal. J. Anal. Appl. Pyrolysis 95, 61–67.
Feng, D., et al., 2018. Improvement and maintenance of biochar catalytic activity for in-situ biomass tar reforming during pyrolysis and $H2O/CO_2$ gasification. Fuel Process. Technol. 172, 106–114.
Fonts, I., et al., 2012. Sewage sludge pyrolysis for liquid production: a review. Renew. Sustain. Energy Rev. 16 (5), 2781–2805.
Fonts, I., La'zaro, M.A., L., Gea, G., Murillo, M.B., 2009. Gas chromatography study of sewage sludge pyrolysis liquids obtained at different operational conditions in a fluidized bed. Ind. Eng. Chem. Res. 48, 5907–5915.
Fragiskos, A.B., Sidiras, D.K., Siontorou, C.G., Bountri, A.N., Politi, D.V., Kopsidas, O.N., Konstantinou, I.G., Katsamas, G.N., Salapa, I.S., Zervopoulou, S.P., 2014. Experimental design for estimating parameter-values of modelling crude oil adsorption on thermochemically modified lignocellulosic biomass. Int. J. Arts Sci 7 (3), 205–222.
Geca, M., Wisniewska, M., Nowicki, P., 2022. Biochars and activated carbons as adsorbents of inorganic and organic compounds from multicomponent systems - a review. Adv. Colloid Interface Sci. 305, 102687.
Han, B., et al., 2013. Co-pyrolysis behaviors and kinetics of plastics–biomass blends through thermogravimetric analysis. J. Therm. Anal. Calorim. 115 (1), 227–235.
He, X., et al., 2018. Effects of pyrolysis temperature on the physicochemical properties of gas and biochar obtained from pyrolysis of crop residues. Energy 143, 746–756.
Huang, H.-j, et al., 2017. Co-pyrolysis of sewage sludge and sawdust/rice straw for the production of biochar. J. Anal. Appl. Pyrolysis 125, 61–68.
Inguanzo, M., et al., 2002. On the pyrolysis of sewage sludge: the influence of pyrolysis conditions on solid, liquid and gas fractions. J. Anal. Appl. Pyrolysis 63 (1), 209–222.
Irwin, R., et al., 2017. Verification of an alternative sludge treatment process for pathogen reduction at two wastewater treatment plants in Victoria, Australia. J. Water Health 15 (4), 626–637.
Ischia, M., et al., 2011. Clay-sewage sludge co-pyrolysis. A TG-MS and Py-GC study on potential advantages afforded by the presence of clay in the pyrolysis of wastewater sewage sludge. Waste Manag. 31 (1), 71–77.
Ji, W., Shen, Z., Wen, Y., 2014. A continuous hydrothermal saccharification approach of rape straw using dilute sulfuric acid. BioEnergy Res. 7 (4), 1392–1401.
Ji, W., Shen, Z., Wen, Y., 2014. A Continuous Hydrothermal saccharification approach of rape straw using dilute sulfuric acid. BioEnergy Res 7, 1392–1401.
Jin, J., et al., 2017. Cumulative effects of bamboo sawdust addition on pyrolysis of sewage sludge: Biochar properties and environmental risk from metals. Bioresour. Technol. 228, 218–226.
Jin, Z., et al., 2018. Co-pyrolysis characteristics of typical components of waste plastics in a falling film pyrolysis reactor. Chin. J. Chem. Eng. 26 (10), 2176–2184.
Jindarom, C., et al., 2007. Thermochemical decomposition of sewage sludge in CO_2 and N2 atmosphere. Chemosphere 67 (8), 1477–1484.
Johansen, J.M., et al., 2011. Release of K, Cl, and S during pyrolysis and combustion of high-chlorine biomass. Energy Fuels 25 (11), 4961–4971.
Lan, K., Qin, Z., Li, Z., Hu, R., Xu, X., He, W., Li, J., 2020. Syngas production by catalytic pyrolysis of rice straw over modified Ni-based catalyst. BioRes 2293–2309.
Lin, Y., et al., 2016. Co-pyrolysis kinetics of sewage sludge and oil shale thermal decomposition using TGA–FTIR analysis. Energy Convers. Manag. 118, 345–352.
Marinos, A.S., Kollia, D., Haralambous, K.-J., Inglezakis, V.J., Moustakas, K.G., Loizidou, M.D., 2007. Effect of acid treatment on the removal of heavy metals from sewage sludge. Desalination 213 (1-3), 73–81.
Mark Siebentritt & Associates, G.O.P.L., Renewable Energy Production from Almond Waste. 2012, Almond Board of Australia Inc.
Martínez, J.D., et al., 2014. Co-pyrolysis of biomass with waste tyres: Upgrading of liquid bio-fuel. Fuel Process. Technol. 119, 263–271.
McNamara, P.J., et al., 2016. Pyrolysis of dried wastewater biosolids can be energy positive. Water Environ. Res 88 (9), 804–810.
Melissa Morris, P.C., Wimmera Bioenergy Resource Audit. 2010, Wimmera Development Association: Victoria.
Mühlbachová, G., 2002. The availability of DTPA extracted heavy metals during laboratory incubation of contaminated soils with glucose amendments. Rostlinná Výroba 48, 536–542.
Park, J.-W., et al., 2019. Fast pyrolysis of acid-washed oil palm empty fruit bunch for bio-oil production in a bubbling fluidized-bed reactor. Energy 179, 517–527.
Patel, S., et al., 2019. Slow pyrolysis of biosolids in a bubbling fluidised bed reactor using biochar, activated char and lime. J. Anal. Appl. Pyrolysis **144**.
Patel, S., et al., 2020. A critical literature review on biosolids to biochar: an alternative biosolids management option. Rev. Environ. Sci. Bio/Technol. 19 (4), 807–841.
Peterson, S.C., 2022. Carbon black replacement in natural rubber composites using dry-milled calcium carbonate, soy protein, and biochar. Processes 10, 1.
, 2018PYREG GmbH, E.R. TECHNOLOGY, Editor. 2018.
Rathnayake, N., et al., 2022. Co-pyrolysis of biosolids with alum sludge: effect of temperature and mixing ratio on product properties. J. Anal. Appl. Pyrolysis **163**.
Ruiz-Gomez, N., et al., 2017. Co-pyrolysis of sewage sludge and manure. Waste Manag. 59, 211–221.
Saleh Khodaparasti, M., et al., 2022. Co-pyrolysis of municipal sewage sludge and microalgae Chlorella vulgaris: Products' optimization; thermo-kinetic study, and ANN modeling. Energy Convers. Manag. **254**.
Sanchez-Reinoso, A.D., Ávila-Pedraza, E.A., Restrepo, H., 2020. Use of Biochar in agriculture. Acta Biol. Colomb. 25 (2), 327–338.
Shahbaz, M., et al., 2020. Investigation of biomass components on the slow pyrolysis products yield using Aspen Plus for techno-economic analysis. Biomass Convers. Biorefin. 12 (3), 669–681.
Shi, W., Liu, C., Shu, Y., Feng, C., Lei, Z., Zhang, Z., 2013. Synergistic effect of rice husk addition on hydrothermal treatment of sewage sludge: fate and environmental risk of heavy metals. Bioresour. Technol. 496–502.
Shuang-quan, Z., et al., 2009. Study of the co-pyrolysis behavior of sewage-sludge/rice-straw and the kinetics. Procedia Earth Planet. Sci. 1 (1), 661–666.
Singh, R.P., Agrawal, M., 2008. Potential benefits and risks of land application of sewage sludge. Waste Manag. 28 (2), 347–358.
Soleha, M.Y., et al., 2016. Characterization of raw and thermally treated alum sludge. Key Eng. Mater. 701, 138–142.
Song, X.D., et al., 2014. Application of biochar from sewage sludge to plant cultivation: Influence of pyrolysis temperature and biochar-to-soil ratio on yield and heavy metal accumulation. Chemosphere 109, 213–220.
Statistics, A.Bo. Agricultural Commodities, Australia, 2017–18. 2019; Available from: https://www.abs.gov.au/AUSSTATS/abs@.nsf/DetailsPage/7121.02017–18?OpenDocument.
Suliman, W., et al., 2016. Influence of feedstock source and pyrolysis temperature on biochar bulk and surface properties. Biomass Bioenergy 84, 37–48.
Svärd, A., Biopolymers and Materials from Rapeseed Straw Biorefining, in Department of Fiber and Polymer Technology. 2018, KTH Royal Institute of Technology: Stockholm, Sweden.
Tantawy, M.A., 2015. Characterization and pozzolanic properties of calcined alum sludge. Mater. Res. Bull. 61, 415–421.
Tufail, T., et al., 2018. Biochemical characterization of wheat straw cell wall with special reference to bioactive profile. Int. J. Food Prop. 21 (1), 1303–1310.
Urych, B., Smoliński, A., 2021. Sewage sludge and phytomass co-pyrolysis and the gasification of its chars: a kinetics and reaction mechanism study. Fuel **285**.
Vasu, H., et al., 2019. Insight into co-pyrolysis of palm kernel shell (PKS) with palm oil sludge (POS): effect on bio-oil yield and properties. Waste Biomass Valoriz. 11 (11), 5877–5889.
Veeken, A.H.M., 1999. Removal of heavy metals from sewage sludge by extraction with organic acids. Water Sci. Technol. 40 (1), 129–136.
Wang, S., et al., 2018. Co-pyrolysis and catalytic co-pyrolysis of Enteromorpha clathrata and rice husk. J. Therm. Anal. Calorim. 135 (4), 2613–2623.
Wang, X., et al., 2016b. Synergetic effect of sewage sludge and biomass co-pyrolysis: a combined study in thermogravimetric analyzer and a fixed bed reactor. Energy Convers. Manag. 118, 399–405.
Wang, X., Zhao, B., Yang, X., 2016a. Co-pyrolysis of microalgae and sewage sludge: Biocrude assessment and char yield prediction. Energy Convers. Manag. 117, 326–334.
Wang, X., C.C, V.W., Li, Z., Song, Y., Li, C., Wang, Y., 2022. Co-pyrolysis of sewage sludge and food waste digestate to synergistically improve biochar characteristics and heavy metals immobilization. Waste Manag. 231–239.
Wang, Z., et al., 2019. Co-pyrolysis of sewage sludge and cotton stalks. Waste Manag. 89, 430–438.
Wang, Z., et al., 2020. Characteristics of biochars prepared by co-pyrolysis of sewage sludge and cotton stalk intended for use as soil amendments. Environ. Technol. 41 (11), 1347–1357.
Yang, X., et al., 2015. Potential method for gas production: high temperature co-pyrolysis of lignite and sewage sludge with vacuum reactor and long contact time. Bioresour. Technol. 179, 602–605.
Yang, Y., et al., 2018. Physicochemical properties of biochars produced from biosolids in Victoria, Australia. Int. J. Environ. Res. Public Health 15, 7.
Yang, Y.Q., et al., 2020. Towards understanding the mechanism of heavy metals immobilization in biochar derived from co-pyrolysis of sawdust and sewage sludge. Bull. Environ. Contam. Toxicol. 104 (4), 489–496.
Zhang, J., et al., 2015b. Multiscale visualization of the structural and characteristic changes of sewage sludge biochar oriented towards potential agronomic and environmental implication. Sci. Rep. 5, 9406.
Zhang, J., et al., 2020. Co-pyrolysis of sewage sludge and rice husk/ bamboo sawdust for biochar with high aromaticity and low metal mobility. Environ. Res 191, 110034.
Zhang, W., et al., 2015a. Beneficial synergetic effect on gas production during co-pyrolysis of sewage sludge and biomass in a vacuum reactor. Bioresour. Technol. 183, 255–258.
Zhao, B., et al., 2017. Surface characteristics and potential ecological risk evaluation of heavy metals in the bio-char produced by co-pyrolysis from municipal sewage sludge and hazelnut shell with zinc chloride. Bioresour. Technol. 243, 375–383.
Zhu, J., et al., 2018. High quality syngas produced from the co-pyrolysis of wet sewage sludge with sawdust. Int. J. Hydrog. Energy 43 (11), 5463–5472.
Zhu, X., et al., 2014. Co-pyrolysis behaviors and kinetics of sewage sludge and pine sawdust blends under non-isothermal conditions. J. Therm. Anal. Calorim. 119 (3), 2269–2279.
Zuo, W., et al., 2014. Characterization of top phase oil obtained from co-pyrolysis of sewage sludge and poplar sawdust. Environ. Sci. Pollut. Res. Int. 21 (16), 9717–9726.